Shock consolidation of Al–Li alloy powders

Li-Hsing Yu
Department of Materials and Metallurgical Engineering, New Mexico Institute of Mining and Technology, Socorro, NM 87801 (U.S.A.)

Marc A. Meyers
Center of Excellence for Advanced Materials, University of California, San Diego, La Jolla, CA 92093 (U.S.A.)

T. C. Peng
McDonnell Douglas Research Laboratories, St. Louis, MO 63166 (U.S.A.)

(Received June 21, 1990; in revised form August 30, 1990)

Abstract

Several rapidly solidified Al–Li-based alloy powders were successfully consolidated into crack-free compacts by explosively generated shock waves. Both flyer plate and direct contact techniques were applied in cylindrical and plate configurations. Densities of the compacted powders reach over 97% of their theoretical values. The microstructures of the compacts were evaluated by optical and electron microscopy. Crack-free compacts were produced by using the flyer tube technique in the cylindrical separated by random stacking faults or several atomic layers of f.c.c. structure. A high density of hot-extruded alloys. Compacts of Al–3wt.%Li–1wt.%Cu–1wt.%Mg–0.2wt.%Zr alloy powders exhibited the highest tensile strength (282 MPa). The optical micrographs showed that the crack-free compacts had considerable interparticle melting. The interparticle melting regions were analyzed by X-ray diffracation and transmission electron microscopy and had a microcrystalline structure with precipitates of δ'-Al_3Li and δ-AlLi. Fractographs of tensile specimens revealed that the compacts having high tensile strength had strong interparticle bonding; their rupture surface exhibited trans-particle fracture.

1. Introduction

Low density and high modulus of elasticity are two unique properties of Al–Li-based alloys. They offer great potential for improved structural efficiency, most desirable for saving weight in aircraft use [1, 2]. The fabrication of Al–Li-based alloys by ingot metallurgy may result in low fracture toughness because of the relatively low rates of solidification, which give rise to unfavorable dispersion of lithium-containing precipitates. Conventional powder metallurgy processing of fully dense aluminum alloys usually includes three steps: canning, degassing and hot extrusion. The long exposure at high temperature will destroy the inherent properties of powder produced by rapid solidification processing. In this research program the Al–Li alloy powders were prepared by inert gas atomization with cooling rates of 10^3–10^5 K s^{-1}; the powders were smaller than 180 μm. Ultrahigh quenching rates minimize chemical segregation and the formation of massive phases and increase the solubility of alloying elements. Therefore the powders produced by this technique have unique microstructures such as microcrystalline or microdendritic structures and metastable phases. These structures greatly contribute to the mechanical properties, but at high temperatures and/or long exposures at moderate temperatures the metastable phases will decompose in the alloys.

Shock consolidation of powders is a technique that successfully retains the microstructures of the initial starting material because it does not require application of external heat. This process uses a combination of high pressures and temperatures within an extremely short time scale to densify powders. The passage of the shock wave

0921-5093/91/$3.50

through the powders leaves a fully dense body behind the shock wave front. Explosive consolidation of powders has been described in the comprehensive monograph by Prümmer [3] as well as in more recent publications [4, 5]. Hard and incompatible powders, which cannot be consolidated with conventional processes [6], can be shock consolidated. It is also becoming an increasingly important method for synthesis of new materials [7].

The purpose of this study was (1) to investigate the feasibility of shock consolidation of Al–Li-based alloy powders in cylindrical and plate configuration by using explosives, (2) to determine the microstructures of consolidated powders by optical, transmission electron and scanning electron microscopy and (3) to compare the mechanical properties with those of products formed by the conventional hot extrusion process.

2. Materials and experimental techniques

The aluminum alloy powders investigated in the research program were produced by inert gas atomization. Figure 1 shows the general morphology of the powder particles and indicates a spherical shape. The chemical composition, mean size and theoretical density for different types of powders are listed in Table 1. The powders were packed in the cylindrical and plate containers after repeated tapping, vibrating for 20 h under vacuum and cold pressing to maximize packing density. Before packing, the powders were stored in an argon atmosphere; loading the powders into the containers was also done in an argon atmosphere.

Two configurations were used for the explosive consolidation experiments: cylindrical and plate configurations. The cylindrical configuration can be divided into (1) the single-tube system [8–10] in which the explosive is in direct contact with the powder container (Fig. 2(a)) and (2) the double-tube system [11–13] in which the powder con-

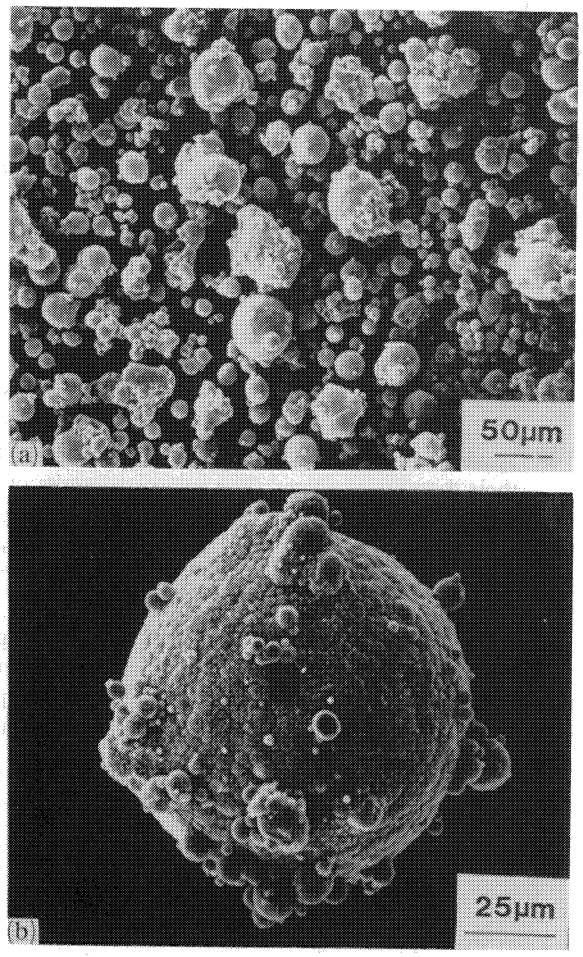

Fig. 1. (a) Scanning electron micrograph of as-received particle. (b) Higher magnification of (a).

TABLE 1

Characteristics of aluminum alloy powders for explosive consolidations

Composition of powder (wt.%)	Geometric mean diameter (μm)		Theoretical density (g cm^{-3})
	By weight	By number[a]	
Al (99.9%)	53	30	2.7
Al–3Li–1Cu–0.2Zr	80	55	2.49
Al–3Li–1Mg–0.2Zr	74	56	2.46
Al–3Li–1Cu–1Mg–0.2Zr	84	58	2.48
Al–4Li–1Cu–1Mg–0.2Zr	96	71	2.45
Al–8.4Fe–7Ce	88	69	2.994

[a]The geometric mean diameter by number is calculated from the measured values of particle size distribution by weight.

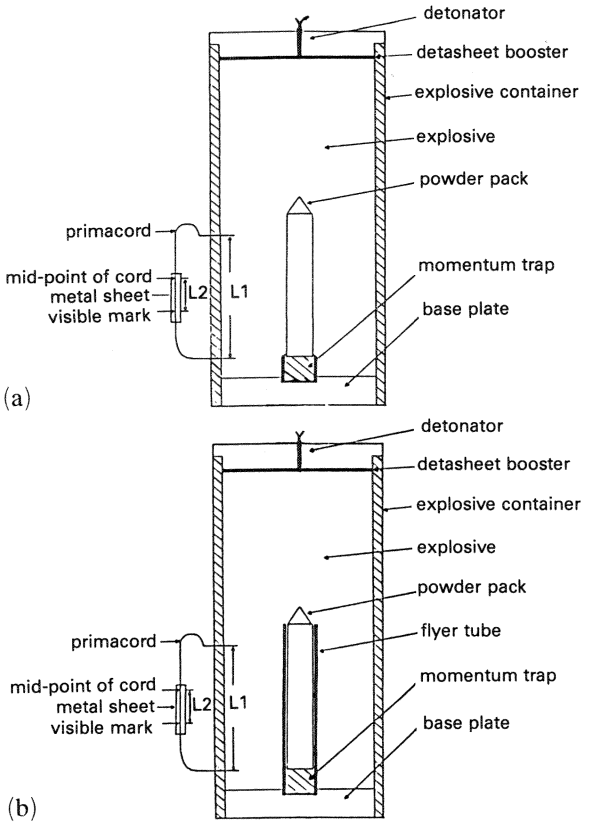

Fig. 2. Experimental arrangement for explosive consolidation of Al–Li-based alloy powders in cylindrical configuration: (a) single-tube system; (b) double-tube system.

tainer is surrounded with a larger diameter steel tube acting as a flyer tube (Fig. 2(b)). The flyer tube is accelerated by the explosive and transmits the shock to the powder. Wilkins [12] suggested that the energy transfer of explosive using a flyer plate is higher and more efficient than using the direct contact method. The experimental conditions used in the cylindrical configurations are listed in Table 2. The plate experiments also used two configurations: (1) the asymmetric sandwich system in which a tamper plate was put on top of the explosive to increase the energy imparted to the flyer plate (Fig. 3(a)) and (2) the open-faced sandwich system in which no tamper plate was used above the explosive (Fig. 3(b)). The experimental conditions for the plate configurations are listed in Table 3. The explosive used was ammonium nitrate–fuel oil (ANFO); the ratio of fuel oil to ammonium nitrate ranged from 4.5 to 11.5 wt.%. The initial pressures were calculated using the impedance-matching technique [14], which is a simple graphical solution procedure. The pressure–particle velocity plot, shown in Fig. 4 [15], is used because the pressure and particle velocity are continuous at the interface. The Hugoniot curve for the powder at a density of 71.5% of the theoretical density was used. This curve is obtained by using the equation of state for the

TABLE 2

Experimental conditions in the cylindrical configurations

Test no.	Composition of powder (wt.%)	Diameter of core (mm)	Composition of explosive (fuel oil in wt.%)	Explosive-to-powder ratio E/M	Packing density (TD%)	Test system (tube)
1	Al–3Li–1Cu–0.2Zr	6.35	ANFO (11.5)	60.8	66.3	Single
2	Al–3Li–1Cu–0.2Zr	6.35	ANFO (11.5)	40.5	66.8	Single
3	Al–3Li–1Cu–0.2Zr	6.35	ANFO (11.5) 12% silica	34.9	71.6	Single
4	Al–3Li–1Cu–0.2Zr	6.35	ANFO (5.8)	34.9	68.3	Double
5	Al–3Li–1Cu–0.2Zr	6.35	ANFO (6.5)	35.6	69.3	Double
6	Al–3Li–1Cu–0.2Zr	6.35	ANFO (6)	34.8	71.4	Double
7	Al–3Li–1Cu–0.2Zr	6.35	ANFO (5.5)	34.0	71.5	Double
8	Al–3Li–1Cu–0.2Zr	6.35	ANFO (5)	34.9	69.6	Double
9	Al–3Li–1Cu–0.2Zr	6.35	ANFO (4.5)	35.2	70.4	Double
10	Al–3Li–1Cu–0.2Zr	6.35	ANFO (5.5)	34.6	68.7	Double
11	Al–3Li–1Cu–0.2Zr	6.35	ANFO (5)	35.2	69.7	Double
12	Al–3Li–1Cu–0.2Zr	None	ANFO (5.5)	31.7	70.4	Double
13	Al–3Li–1Cu–0.2Zr	9.53	ANFO (5.5)	36.1	70.0	Double
14	Al–3Li–1Cu–0.2Zr	3.18	ANFO (5.5)	33.4	72.0	Double
15	Al (99.9%)	6.35	ANFO (5.5)	42.7	52.0	Double
16	Al–3Li–1Cu–1Mg–0.2Zr	6.35	ANFO (5.5)	36.8	64.4	Double
17	Al–4Li–1Cu–1Mg–0.2Zr	6.35	ANFO (5.5)	37.4	64.9	Double
18	Al–8.4Fe–7Ce	6.35	ANFO (5.5)	29.7	66.9	Double
19	Al–3Li–1Mg–0.2Zr	6.35	ANFO (5.5)	36.5	67.6	Double
20	Al–8Fe–4Ce	6.35	ANFO)5.5)	32.0	63.0	Double
21	Al–3Li–1Cu–0.2Zr[a]	6.35	ANFO (5.5)	37.0	66.3	Double

[a]Heat treated at 510 °C for 6 h in vacuum and slow cooled to 25 °C.

powder, calculated using the Mie–Gruneisen procedure [11]. For the alloy used in test 7, the equation of state for the solid alloy (Al–3wt.%Li–1wt.%Cu–0.2wt.%Zr) is

$$U_s = 5.29 + 1.33 U_p \quad (\mathrm{km\ s^{-1}})$$

where U_s and U_p are the shock and particle velocities respectively. The Gruneisen constants and other parameters needed were obtained from the *LASL Shock Hugoniot Data* compilation [15]. Averaging was done based on the mean fractions of the constituents. The velocity of the explosively accelerated flyer tube was calculated by using a modified Gurney equation [11] and was found to be 1.7 km s^{-1}. The impact produces a pressure of 38 GPa in the steel containers. This is found by the impedance-matching technique, a technique commonly used in shock wave calculations and graphically represented in Fig. 4. Applying the impedance-matching technique again, one obtains a pressure of 10 GPa in the powder.

The structure of the compacts was studied by optical, scanning electron and transmission

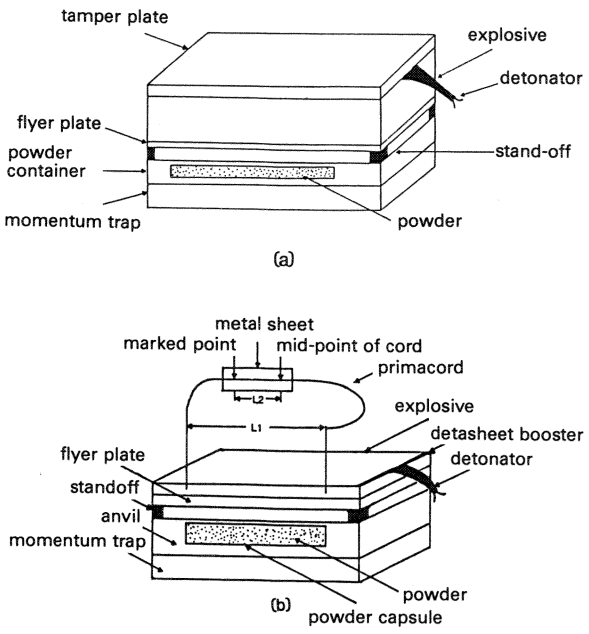

Fig. 3. Experimental arrangement for explosive consolidation of Al–Li-based alloy powders in plate configuration: (a) asymmetric sandwich; (b) open-faced sandwich (with Dautriche system for measuring velocity).

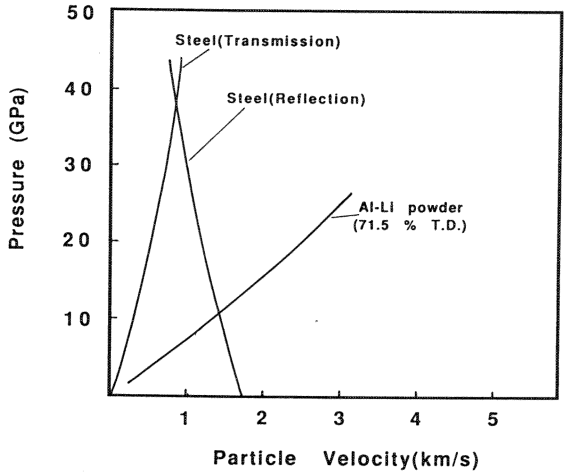

Fig. 4. Graphic solution for initial pressure induced to target by using impedance-matching technique [12].

TABLE 3

Experimental conditions in the plate configurations

Test no.	Experimental geometry	Flyer plate thickness (mm)	Composition of explosive (fuel oil in wt.%)	Explosive-to-powder ratio E/M	Packing density (TD%)
22	Asymmetric	3.175	ANFO (6)	12.7	72.5
23	Asymmetric	3.175	ANFO (6)	6.7	61.0
24	Asymmetric	3.175	ANFO (6)	4.6	61.0
25	Open-faced	3.175	ANFO (6)	4.0	61.0
26	Asymmetric	3.175	ANFO (11.5)	4.5	64.6
27	Asymmetric	6.35	ANFO (6)	9.8	66.0
28	Asymmetric	3.175	ANFO (6)	4.3	66.0
29	Asymmetric	6.35	ANFO (6)	4.7	61.0
30	Asymmetric	6.35	ANFO (6)	5.6	62.0
31	Asymmetric	6.35	ANFO (6)	4.2	67.0

1. The compositions of powder in the 10 specimens are all the same: Al–3Li–1Cu–1Mg–0.2Zr (in wt.%).
2. The size of all the tamper plates (steel) in the asymmetric sandwich geometry is 457.2 mm × 340.8 mm × 12.7 mm.
3. The powder containers and momentum traps of tests 22–27 were made of aluminum alloy; those of tests 28–31 were made of steel.
4. The size of all the powder containers and momentum traps was 457.2 mm × 340.8 mm × 12.7 mm.

electron microscopy. X-ray diffractometry was used to analyze the phases of compacts. The tensile tests were conducted at McDonnell Douglas Research Laboratory at ambient temperature.

3. Results and discussion

Thirty-one experiments were conducted using both cylindrical and plate configurations in this program. In the single-tube system the powder particles underwent considerable deformation and were interlocked together; the input energy was not sufficient to produce interparticle bonding or melting among powder particles. The radial and circumferential cracks shown in Fig. 5 were found in the cross-sections of compacts from tests 2 and 3 respectively. These cracks indicate that the compacts did not have sufficient interparticle bonding to accommodate the tensile stresses which are caused by rarefaction waves.

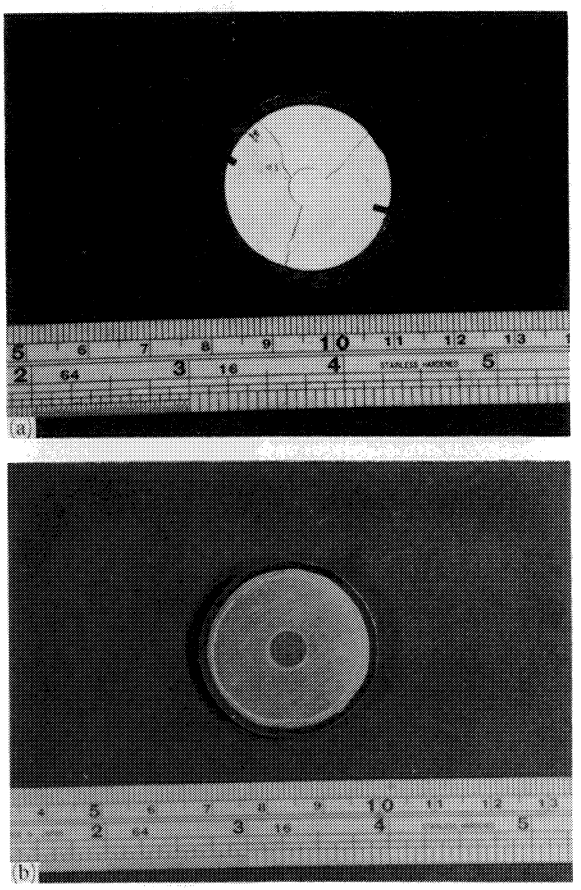

Fig. 5. Cross-sections of compacts (a) and test 2 and (b) from test 3.

An additional reason is the different pulse shapes produced for the single-tube and flyer tube techniques. The powder particles were easily pulled out by grinding or polishing and formed voids, as shown in Fig. 6 (arrows indicate voids). The predominant fracture mode of compact in the single-tube system was interparticle rupture, as shown in Fig. 7(a). The microcracks present along the boundaries between the particles should be the initial origin of the fracture. The higher magnification fractograph (Fig. 7(b)) shows that the particles were heavily deformed, formed many facets and interlocked with each other.

In the double-tube system, most compacts could reach over 97% of the theoretical density without cracking. Figure 8 shows the cross-section of the compact of test 7. No cracking is seen. The optical micrograph (Fig. 9) shows that considerable interparticle melting (dark areas) occurred in the compact. The fractograph (Fig. 10) shows a dimpled appearance. The tensile strength of this compact was higher than that of compacts in the single-tube system. The scanning electron micrograph of the polished and etched surface of the compact is shown in Fig. 11. The interparticle melting regions are indicated by an arrow. The microstructural modifications resulting from shock consolidation were analyzed by transmission electron microscopy. Figure 12(a) shows a bright field image of the specimen. The interparticle melting region is on the side of the electropolished hole in the thin foil specimen. Figure 12(b) is the selected area diffraction

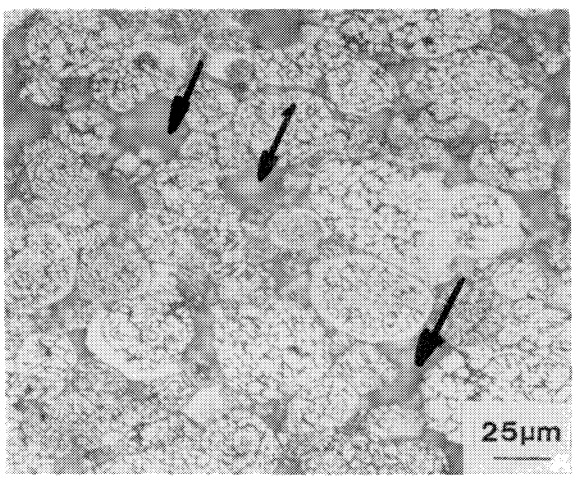

Fig. 6. Optical micrograph of compact from test 2.

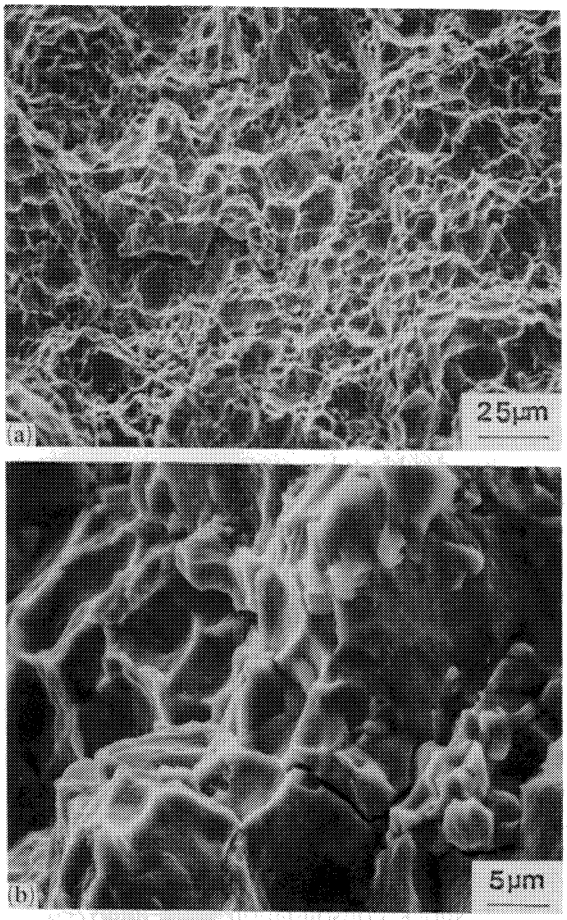

Fig. 7. (a) Scanning electron micrograph of the fracture surface from test 2. (b) Higher magnification of (a).

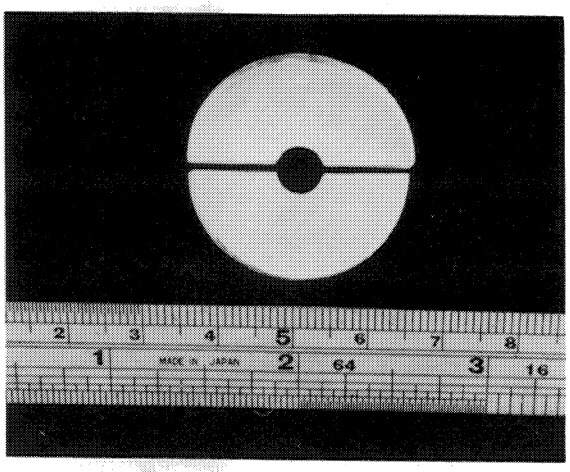

Fig. 8. Cross-section of compact from test 7.

pattern in the interparticle region. The extremely fine-grained nature of the microstructure is reflected in the diffraction pattern, which shows a series of concentric, spotty rings. A higher mag-

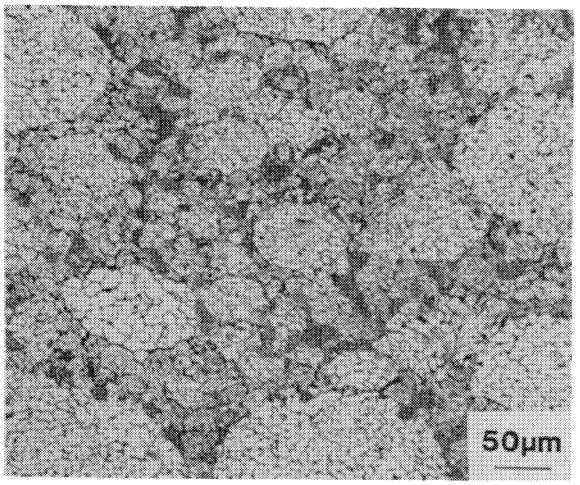

Fig. 9. Optical micrograph of compact from test 7.

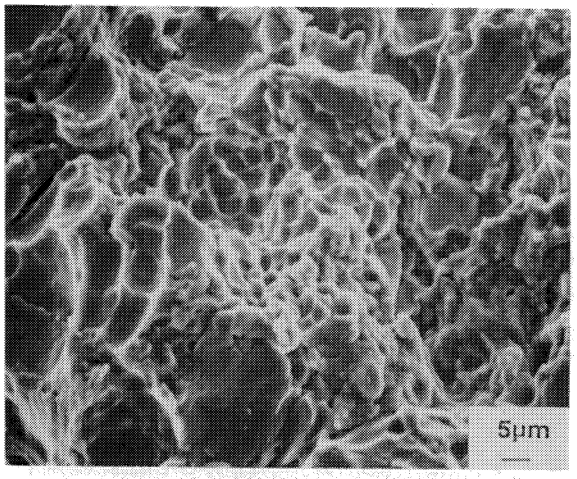

Fig. 10. Scanning electron micrograph of the fracture surface from test 7.

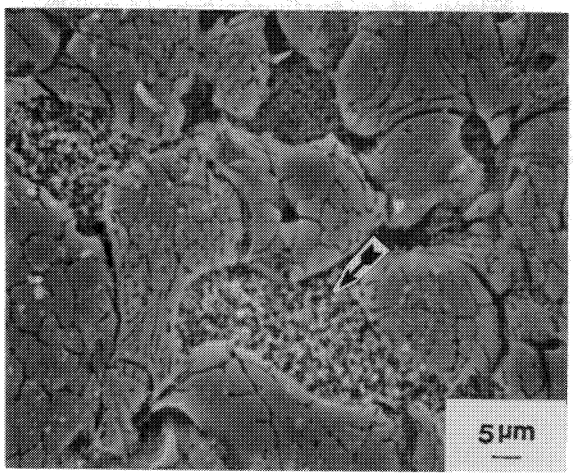

Fig. 11. Scanning electron micrograph of the polished and etched surface of compact from test 7.

nification bright field image (Fig. 13(a)) shows some precipitates existing at the grain boundaries. The selected area diffraction pattern obtained from the coarse-grained region (Fig. 13(b)) shows superlattice reflections. This diffraction pattern was analyzed and the precipitate was determined to be δ'-Al_3Li phase. The X-ray diffraction patterns of as-received powders before and after shock consolidation are shown in Fig. 14. Some small peaks could be found besides the two higher peaks after consolidation. These peaks were analyzed to be δ'-Al_3Li and δ-AlLi. The results indicate that the consolidated powders have undergone some microstructural modification.

In the compact of test 21 the powders were heat treated at 510 °C for 6 h in vacuum and slowly cooled to 25 °C before packing into the

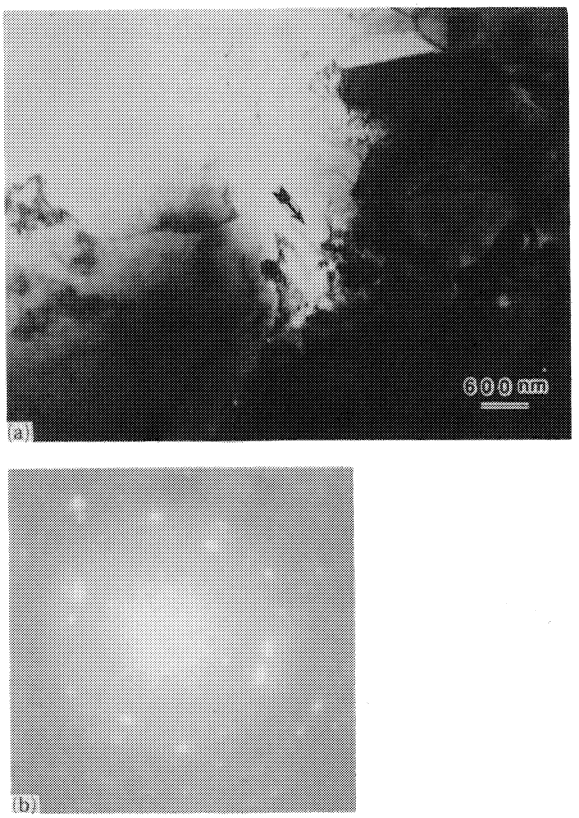

Fig. 12. (a) Bright field image of compact from test 7. (b) Selected area diffraction pattern in interparticle region where arrow points in (a).

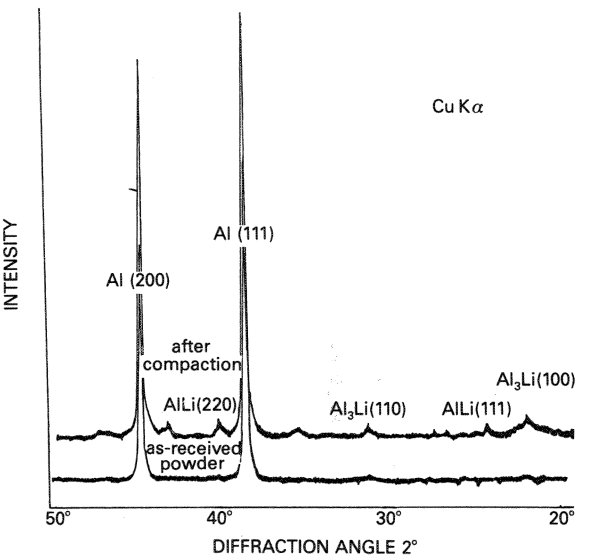

Fig. 14. Diffraction patterns for as-received powders and compact from test 7.

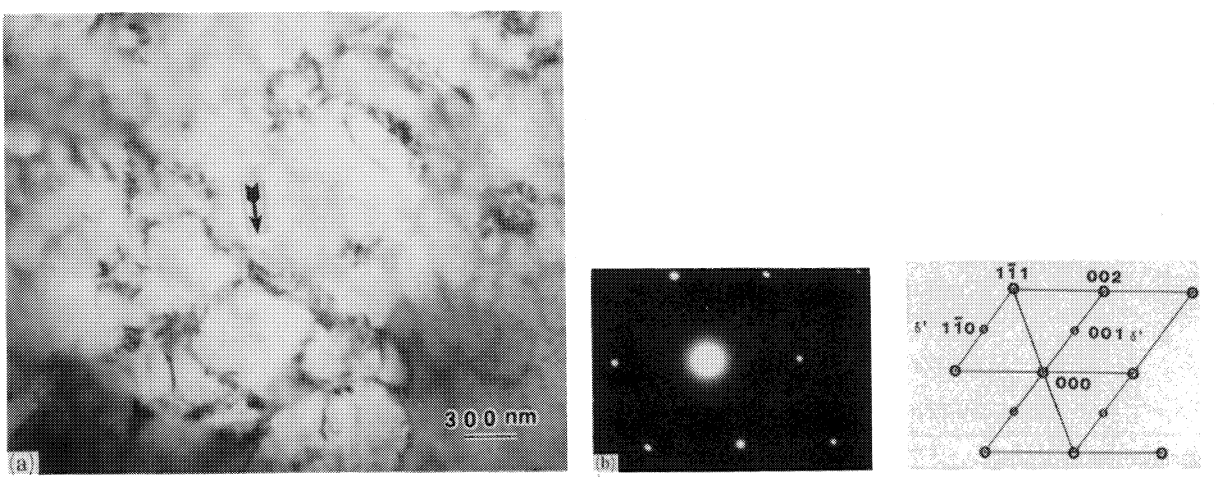

Fig. 13. (a) Bright field image of particle interior region. (b) Selected area diffraction pattern in region where arrow points in (a).

container. The fracture surface morphology (Fig. 15) observed is dimpled. It is thought that a ductile material was formed by interparticle melting and resolidification. In the plate configuration the appearance of the compact after removal from the container is shown in Fig. 16. The fracture surface of the compact presented a similar appearance to that in the single-tube system, but more microcracks and voids existed between the particles. The poor consolidation of the compact and the existence of microcracks result in low strength.

The mechanical properties of compacts with different powder compositions are listed in Table 4. Compacts with different powder compositions had different tensile strengths. The compact of Al–3wt.%Li–1wt.%Cu–1wt.%Mg–0.2wt.%Zr alloy had the highest tensile strength, 282 MPa. The tensile strength (256 MPa) of the Al–8.4wt.%Fe–7wt.%Ce compact was equal to 89% of the tensile strength of the extruded sample. The 99.9 wt.% Al compact had a tensile strength of 74.5 MPa. This indicates that the initial material property has an important effect on the mechanical strength of the shock-consolidated material. The tensile strength (265 MPa) of the Al–3wt.%Li–1wt.%Cu–0.2wt.%Zr compact with preshock treatment was equal to 87% of the tensile strength of the extruded sample. The tensile strengths of compacts with the same compositions but without preshock heat treatment were approximately 180 MPa. This indicates that the preshock heat treatment seems to have a beneficial effect on the mechanical property for shock consolidation. The cylinder of 99.9 wt.% Al compact had a deep conical void along the central axis in the longitudinal direction. The powders were totally molten under this experi-

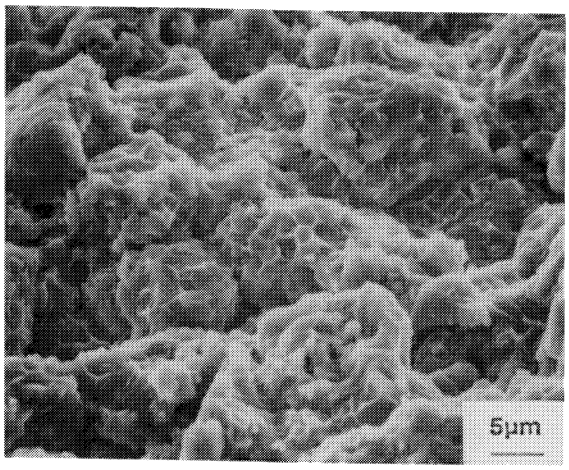

Fig. 15. Scanning electron micrograph of the fracture surface from test 21.

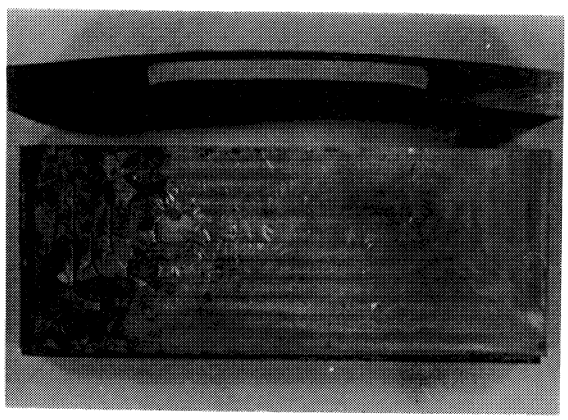

Fig. 16. Section of planar container from test 31.

TABLE 4

Experimental results for different aluminum alloy powder compositions in double-tube system

Test no.	Composition of powder (wt.%)	Detonation velocity (km s^{-1})	Consolidated density (% TD)[a]	Tensile strength (MPa)[b]	Tensile strength of extruded sample (MPa)[b]
15	Al (99.9%)	3.59	100	74.5	100
16	Al–3Li–1Cu–1Mg–0.2Zr	3.47	99	282	—
17	Al–4Li–1Cu–1Mg–0.2Zr	3.87	97.5	207	—
18	Al–8.4Fe–7Ce	3.72	99	256	287
19	Al–3Li–1Mg–0.2Zr	3.45	99.6	175	—
20	Al–8Fe–4Ce	3.70	99.6	154	—
21	Al–3Li–1Cu–0.2Zr[c]	3.59	100	265	305

[a]TD is theoretical density.
[b]Measured values (McDonnell Douglas Research Laboratories).
[c]Heat treated at 510 °C for 6 h in vacuum and slow cooled to 25 °C.

mental condition. Thus the original material properties play a very important role in the shock consolidation; pure and ductile metals are more easily shock consolidated than their harder alloys.

4. Conclusions

It was demonstrated that Al–Li alloy powders can be shock consolidated. Sound compacts were produced and the microstructural features of rapid solidification could be retained.

(1) Densities of the shock-consolidated Al–Li-based alloy powders reached over 97% of their theoretical values.

(2) The flyer tube technique (the double-tube system) produced sound compacts without cracking. The higher pressure and longer pulse duration in the powder established by the flyer tube technique are responsible for the improved properties.

(3) Minor changes of powder composition observed did not affect the densification and interparticle bonding. These compacts all exhibited good consolidation and considerable tensile strengths.

(4) The powder with preshock heat treatment responds very well to shock consolidation. The tensile strength of the compact was equal to 87% of the tensile strength of the extruded material.

(5) While the 99.9 wt.% Al powder underwent complete melting, higher strength powders showed less melting. This shows that the mechanical strength of the powder is an important parameter in shock consolidation.

(6) Transmission electron microscopic observations showed that the interparticle melting region has a microcrystalline structure with precipitates of $\delta'Al_3Li$ and δ-AlLi, among others.

(7) Scanning electron microscopic observations showed different rupture modes dependent on the consolidation parameters. The different rupture modes are related to the degree of bonding between particles. Interparticle fracture is evidence of the weak bonding between particles; the fracture progresses along the boundaries of particles. Transparticle fracture is evidence of strong bonding between particles (stronger than the particles themselves); the fracture passes through the interior of particles.

(8) Heat treatment of powders prior to shock consolidation resulted in an improvement of the mechanical properties.

Acknowledgments

This research was supported by McDonnell Douglas Research Laboratories. The authors would like to thank Dr. Charles Whitsett for his financial help. The help of Mr. D. Hunter and of the staff of TERA which provided assistance in the shock consolidation experiments is greatly appreciated. Professor K. K. Chawla provided help and encouragement throughout this research. The use of the facilities of the Center of Excellence for Advanced Materials is gratefully acknowledged.

References

1 T. H. Sanders Jr. and E. A. Starke Jr., *Foote Prints, 44* (1981) 11.
2 T. H. Sanders Jr. and E. A. Starke Jr., in T. H. Sanders Jr. and E. A. Starke Jr. (eds.), *Aluminum–Lithium Alloys II*, TMS–AIME, Warrendale, PA, 1984, p. 1.
3 R. Prümmer, *Explosivverdichtung Pulvriger Substanzen*, Springer, Berlin, 1987.
4 M. A. Meyers, N. N. Thadhani and L.-H. Yu, in L. E. Murr (ed.), *Shock Waves for Industrial Applications*, Noyes, Park Ridge, NJ, 1988, p. 265.
5 R. Prümmer, *Mat.-wiss. Werkstofftech., 20* (1989) 410.
6 R. B. Schwarz, P. Kasiraj, T. Vreeland Jr. and T. J. Ahrens, *Acta Metall., 32* (1984) 1243.
7 R. A. Graham, B. Morosin, Y. Horie, E. L. Venturini, M. Boslough, M. J. Carr and D. L. Williamson, in Y. M. Gupta (ed.), *Shock Waves in Condensed Matter*, Plenum, New York, 1986, p. 693.
8 T. C. Peng, S. M. L. Sastry, J. E. O'Neal and D. T. Brasher, *Metall. Trans. A, 16* (1985) 1445.
9 M. A. Meyers, L. E. Murr and B. B. Gupta, *J. Met., 33* (1981) 21.
10 M. L. Wilkins, Dynamic powder compaction, *Lawrence Livermore National Laboratory Rep. 90142*, 1983.
11 M. A. Meyers and S. L. Wang, *Acta Metall., 36* (1988) 925.
12 M. L. Wilkins, in I. Berman and J. W. Schroeder (eds.), *High Energy Rate Fabrication—1984, San Antonio, TX, 1984*, ASME, p. 63.
13 S. L. Wang, Explosive consolidation of nickel-base superalloy powders, *Ph.D. Dissertation*, New Mexico Tech, Socorro, NM, 1986.
14 O. E. Jones, in L. Davidson *et al.* (eds.), *Behavior and Utilization of Explosives in Engineering Design*, ASME, New Mexico Section, Albuquerque, NM, 1972, p. 125.
15 S. P. Marsh (ed.), *LASL Shock Hugoniot Data*, University of California Press, Berkeley, CA, 1980, pp. 57, 104, 158, 165.